Anodic Stress Corrosion Cracking Suspectibility of Nickel and Nickel-Chromium Alloys Containing Molybdenum and Iron in Bicarbonate Plus Chloride Solutions at 90°C

N.S. Zadorozne,[‡,,***,**] C.M. Giordano,[**,****] R.B. Rebak,[****] A.E. Ares[*] and R.M. Carranza[**,***]*

ABSTRACT

It is reported in the literature that alloy C-22 (N06022) was found to be susceptible to stress corrosion cracking (SCC) in presence of bicarbonate ions, at temperatures higher than 60°C and anodic applied potentials in the order of 400 mV_{SCE}, (where SCE is the saturated calomel electrode) *when using slow strain rate tests (SSRTs). This potential range of cracking susceptibility was associated with the instability of a film that may form on the surface. In order to elucidate the role of the alloying elements on the SCC susceptibility of nickel (Ni)-based alloys, four alloys—C-22 (N06022), 600 (N06600), 800H (N08800) and Ni-201 (N02201)—were tested under the same conditions. Results showed that even though C-22, 600, and 800 may have similar electrochemical anodic behavior, only C-22 may present a clear case of SCC at anodic potentials.*

KEY WORDS: bicarbonate, chloride, chromium, nickel alloys, stress corrosion cracking

INTRODUCTION

Stress Corrosion Cracking of Nickel and Nickel-Based Alloys

In general, nickel (Ni)-based alloys are resistant to corrosion and stress corrosion cracking (SCC) because Ni can dissolve a large amount of beneficial alloying elements while still maintaining excellent mechanical properties. One of the advantages of Ni alloys over austenitic stainless steels is the resistance of the Ni alloys to chloride-induced SCC, which chronically limits the performance of the austenitic stainless steels in many industrial applications. That is, Ni and Ni alloys with more than 40% of Ni are practically immune to chloride-induced environmental cracking.[1] However, Ni alloys suffer environmentally assisted cracking in other environments, such as highly caustic, wet hydrofluoric acid (HF) upstream oil and gas exploration and production, supercritical water oxidation application processes, and high-temperature water that is typical of light-water reactors normal operating conditions.[1-2]

The environmentally assisted cracking behavior of high-Ni alloys (such as X-750, 800, 600, and 690) has been extensively studied in the last 50 years regarding their use in commercial light-water reactors in the vicinity of 300°C.[3-5] The susceptibility of Ni alloys to environmental cracking in nuclear reactors is a strong function of the alloy composition and yield strength (cold work), as well as on the environmental conditions such as temperature, water chemistry, degree of damage by irradiation, corrosion potential (e.g., controlled by hydrogen gas), etc.[6-11]

Submitted for publication: April 25, 2014. Revised and accepted: October 11, 2014. Preprint available online: November12, 2014, http://dx.doi.org/10.5006/1326.

‡ Corresponding author. E-mail: nataliazadorozne@gmail.com.
* Instituto de Materiales de Misiones - IMAM (CONICET – Universidad Nacional de Misiones - UNaM). Félix de Azara 1552.(3300) Posadas-Misiones.
** Gerencia Materiales, CNEA, Av. General Paz 1499, (B1650KNA) San Martín, Buenos Aires, Argentina.
*** Instituto Sabato – UNSAM/CNEA, Av. General Paz 1499 (B1650KNA) San Martín, Buenos Aires, Argentina.
**** GE Global Research, 1 Research Circle, CEB2551, Schenectady, NY 12309, USA.

ISSN 0010-9312 (print), 1938-159X (online)
15/000071/$5.00+$0.50/0

Because of their excellent resistance to environmentally assisted cracking, the use of Ni alloys in oil and gas production is growing because of the increasingly harsh conditions of some wells.[12] The most common Ni alloys used in oil and gas are thermally treated high-strength material such as alloys 718 and 625. The use of Ni alloys in oil and gas production is still limited because of their unavailability and higher cost.[12]

The environmentally assisted cracking of commercially pure Ni was investigated mainly because of its application in the handling of caustic environments at higher temperatures. Both intergranular and transgranular cracking of crystalline Ni was reported during slow strain rate tests (SSRTs) of cold drawn rods of Ni-200 at cathodic applied potentials.[13] It was postulated that zero valent lithium (Li) was responsible for the cracking of Ni-200 under the tested conditions.[13] Intergranular cracking of strips of Ni, with a composition similar to Ni-200, produced via powder metallurgy and cast plus wrought after precharging with hydrogen (H) for 24 h in 1 N sulfuric acid (H_2SO_4) and then bent in air.[14] Intergranular embrittlement of Ni-200 and Ni-201 were also reported for H_2SO_4 cathodically charged specimens and for thermally charged in high-pressure H_2 specimens.[15-16]

Using U-bend specimens, cracking of nickel-copper (Ni-Cu), nickel-chromium-iron (Ni-Cr-Fe), and nickel-chromium-molybdenum (Ni-Cr-Mo) alloys were reported in the presence of vapor phase and liquid phase wet HF.[17-18] Environmentally assisted cracking was also reported in alloy G-30, which was in service in a HF environment.[19]

Ni-Cr-Mo Alloys for Nuclear Waste Applications

Alloy C-22 (Ni-22% Cr-13% Mo-3% W-3%Fe; W is tungsten) was designed to resist corrosion in industrial environments for both oxidizing and reducing applications.[20-23] Because of these excellent properties, it is one of the candidates for the corrosion resistant barrier of high-level nuclear waste containers.

Disposal in stable geological formations is the strongest worldwide alternative for managing high-level nuclear waste.[24-28]

Geological repositories are based on the multi-barrier principle (defense in depth), which consists of bringing a number of barriers (natural and engineering) between the waste and the biosphere. The engineered barriers are specifically designed to prolong the isolation of waste and limit the potential for release of radionuclides.[24-28] The main engineering barrier is the container for the waste.

Containers will serve in natural environments characterized by multi-ionic aqueous solutions.[24-30] It is estimated that the life of the corrosion-resistant barrier of the container could be reduced because of SCC.[28,31]

The SCC susceptibility of alloy C-22 has been studied in a variety of media and conditions.[32-44] Alloy C-22 was found to be resistant to cracking in pure chloride (Cl^-) environments.[19,32] However, alloy C-22 was found susceptible to SCC in a potential range between 0.3 V_{SCE} and 0.4 V_{SCE} in simulated concentrated groundwater containing Cl^-, carbonate (CO_3^{-2}), and bicarbonate (HCO_3^-) above 65°C.[32-44]

The studies also suggest that the coexistence of HCO_3^- and Cl^- ions is particularly damaging to the resistance of alloy C-22 to SCC. Pure HCO_3^- solutions would cause SCC, but the susceptibility appears to increase with increasing Cl^- concentration in the presence of HCO_3^-.[29-37]

It was found experimentally that SCC will occur in a pH range between 8.5 and 10.5.[42] It has been suggested that the susceptibility to SCC could be related to the occurrence of an anodic peak in the polarization curves in these media.[35-42]

Dunn, et al., showed that when alloy C-22 suffers SCC in HCO_3^- containing Cl^- solutions, a thick anodic film is observed on the alloy surface and Cr in the film is depleted with respect to the base alloy. They suggested causality between these experimental facts.[42]

Recently, Mishra, et al.,[44-45] observed an anodic peak in chloride solutions containing bicarbonate for Hybrid BC-1[†] (a Ni-Cr-Mo alloy), which was confirmed by x-ray photoelectron spectroscopy (XPS) analyses that, at a lower potential, prior to the current increase, the surface is covered by a thin oxide with high Cr (III) oxide (Cr_2O_3)content and containing Mo in several oxidation states.[44-45] They also showed that the current increase is accompanied by the loss of Cr and Mo leading to a film that is effectively Ni hydroxide [$Ni(OH)_2$] containing small amounts of Ni oxide (NiO).[44-45]

The purpose of the present work was to use potentiodynamic polarization curves and SSRT to further evaluate the contribution of the anodic peak on the SCC susceptibility of alloy C-22 in media containing HCO_3^- and Cl^- ions, at 90°C. The tests were conducted using specimens of different Ni alloys: C-22 (Ni-Cr-Mo), 600 (Ni-Cr-Fe), 800H (Ni-Fe-Cr), and 201 (99.5% Ni).

EXPERIMENTAL

The specimens for electrochemical and SCC tests were prepared from mill annealed 1 in (2.54 cm) commercial bar stock alloys.

The chemical composition of the material used in this study is provided in Table 1. The Ni-based alloys used in this work have a face-centered cubic (fcc) structure.

The electrochemical response of the alloys was evaluated using potentiodynamic polarization curves.

[†] Trade name.

TABLE 1
Actual Composition of Nickel Alloys

Alloy	Actual Composition (wt%)								
	Ni	Cr	Mo	W	Fe	Si	Mn	C	Others
C-22 (N06022)	56.58	22.26	13.90	3.15	3.81	0.02	0.24	0.004	0.2Co
600 (N06600)	73.44	16.56	—	—	8.83	0.27	0.24	0.06	0.253Al
800H (N08810)	31.49	20.92	—	—	44.89	0.28	1.03	0.09	0.49Al 0.57Ti
201 (N02201)	99.50	—	—	—	0.11	0.10	0.23	0.02	0.03Co

The specimens used were in the form of parallelepipeds, a variation of the ASTM G5[46] specimen, with approximate dimensions of 12 by 12 by 15 mm. The exposed area to the solution was approximately 10 cm^2. The specimens had a finish grinding of abrasive silicon carbide (SiC) paper #600, and were degreased in acetone and washed in distilled water within the hour prior to testing. All the electrochemical tests were conducted in a 1 L, three-electrode vessel. Nitrogen (N_2) was purged through the solution 1 h prior to testing and was continued throughout the entire test. A water-cooled condenser combined with a water trap was used to avoid evaporation of the solution and to prevent the ingress of air (oxygen). The temperature of the solution was controlled by immersing the cell in a water bath, which was kept at a constant temperature. The reference electrode was a saturated calomel electrode (SCE), which had a potential of 0.242 V more positive than that of the standard hydrogen electrode. The reference electrode was connected to the solution through a water-cooled Luggin probe; the reference electrode was kept at room temperature. The electrode potentials were not corrected for the thermal liquid junction potential because it was assumed to be on the order of a few millivolts.[47] The counter-electrode consisted of a flag of platinum (Pt) foil (total area 50 cm^2) spot-welded to a platinum wire. All the potentials in this paper are reported in the SCE scale. The scan rate used was 0.167 mV/s and the scan was initiated after the application of a constant cathodic current density of 50 $\mu A/cm^2$ during 5 min (cathodic pretreatment) starting at the final potential of the cathodic step until an anodic current density of ~3 mA/cm^2 was reached, which was the end of the test. The tests were performed in duplicate in a 1.148 mol/L sodium bicarbonate ($NaHCO_3$) + 1.5 mol/L sodium chloride (NaCl) solution at 90°C.

Results of the anodic polarization test were linked to the SCC susceptibility results determined using SSRT.

The SSRT was conducted in accordance with the ASTM G129 procedure.[48] The SSRT specimens were machined from rods of Ni-based alloys. All specimens were cylindrical, approximately 150 mm in length and 2.5 mm diameter. The initial strain rate used in the tensile tests was 1.6×10^{-6} s^{-1}. This deformations rate is similar to that used by other authors.[37-40]

Before starting the tests, the specimens were longitudinally polished with #600 abrasive papers. The test conditions were: 1.148 mol/L $NaHCO_3$ + 1.5 mol/L NaCl at 90°C and with applied potentials of 200 mV_{SCE}, 300 mV_{SCE}, and 400 mV_{SCE} to determine if there was a direct correlation between the anodic peak in the polarizations tests and the susceptibility to cracking in the SSRTs.

Post-test examination was performed using optical and scanning electron microscopy (SEM).

RESULTS AND DISCUSSION

The potentiodynamic polarization curves of alloys C-22, 600, 800H, and 201 in 1.148 mol/L $NaHCO_3$ + 1.5 mol/L NaCl at 90°C are presented in Figure 1. The solution at room temperature before starting the polarization experiments and in naturally aerated conditions had a pH of 8. Once the test has been finished, it was found that the pH increased to 10 measured in the same conditions as the first pH measurement.

An anodic peak is observed at ~300 mV_{SCE} for alloy C-22 (Figure 1). At potentials beyond this peak, a pseudo-passive behavior is observed in the potential range of ~400 to 700 mV_{SCE}. Alloy 600 showed a similar behavior as alloy C-22. Alloy 800H showed a smaller passive zone compared with alloys C-22 and 600 and then showed two peaks prior to the transpassive zone. The first well-defined peak occurred at a potential close to 75 mV_{SCE}. The second less-defined or more-rounded peak appeared at potentials similar to the potentials of the peaks in alloys C-22 and 600.

Alloy 201 showed an active-to-passive transition peak followed by a passive range with a current density one order of magnitude higher than for the Cr containing alloys (Figure 1). This active peak in Ni-201 was not observed in alloys C-22, 600, and 800H, probably because of the presence of Cr in them.

As additional information, the corrosion potential (E_{corr}) was recorded over time in a solution of 1.148 mol/L $NaHCO_3$ + 1.5 mol/L NaCl at 90°C under aerated conditions. Figure 2 shows these results. After the elapsed time, the corrosion potential of alloy C-22 reached a value of –352 mV_{SCE}, while alloys 600, 800H, and 201 recorded values of –366 mV_{SCE}, –385 mV_{SCE}, and –644 mV_{SCE}, respectively.

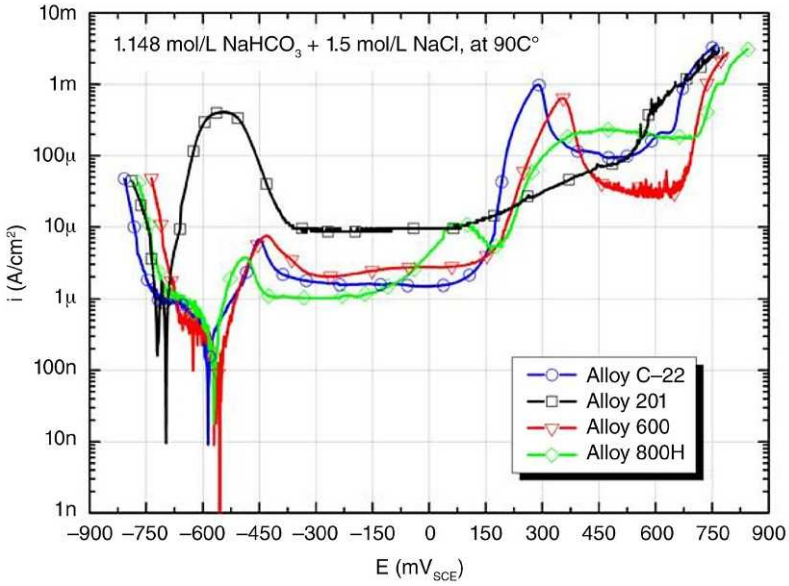

FIGURE 1. *Potentiodynamic polarization curves of alloys C-22, 600, 800H, and 201 in 1.1 mol/L $NaHCO_3$ + 1.5 mol/L NaCl at 90°C. (20%CW carbon steel)*

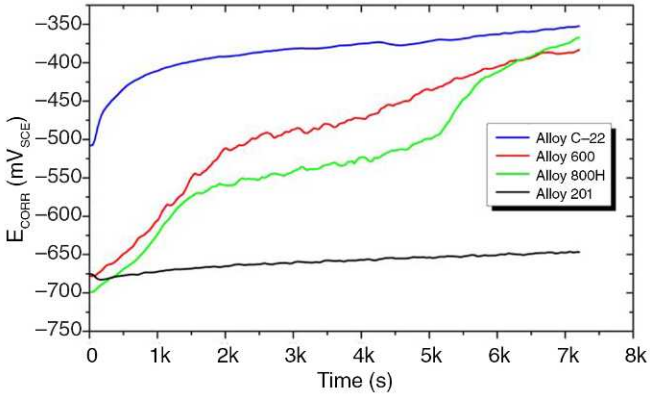

FIGURE 2. *Variation of E_{corr} versus time in 1.148 mol/L $NaHCO_3$ + 1.5 mol/L NaCl at 90°C in aerated conditions.*

Table 2 and Figures 3 through 6, show the results from the straining tests. The stress in Figures 3 through 6 was calculated using the initial cross sectional area of the specimens. The values of area reduction, rupture times, maximum stress, elongation to rupture in the environment and percentage of SCC in the fracture surface, are compared with the results of the tested specimens in air, at room temperature (control test), using parameters such as reduction in area ratio (RRA = RA_e/RA_c), time to failure ratio (RTTF = TTF_e/TTF_c), tensile strength ratio (RTS = TS_e/TS_c) and elongation radio (RE = E_e/E_c). In Figure 7, the parameters for the four alloys studied in this work are compared. The suffix "e" represents the environmental, while the suffix "c" stands for test control, (as defined in the G129 standard). It can be seen that the time to rupture, the maximum load and the reduction of area decreased as the applied potential increased. This behavior is clearly observed for alloy C-22.

Alloy 201 showed a high rate of generalized corrosion when exposed to the environment, which could have masked any trace of cracks (Figure 3). Because of the severe general corrosion, the SSRT curves differ significantly from each other, making it impossible to extract useful information. When the applied potential was higher, the surface of the specimen was covered by a green, loose, porous corrosion product. Considering the pH and applied potentials, this film could be composed of NiO or $Ni(OH)_2$.[49] The general corrosion damage of Ni-201 was also observed in the images obtained by SEM (Figures 8 through 10). It can be observed that the specimens were severely damaged by generalized corrosion at the highest anodic applied potentials.

Alloy 800H showed a different behavior from Ni-201. Tensile curves for alloy 800H obtained at potentials of 300 and 200 mV_{SCE} showed only a slight decrease in failure times and maximum loads relative to the control test in air (Figure 4) indicating that at the two lowest applied potentials, alloy 800H did not suffer severe dissolution nor cracking. However, the test at 400 mV_{SCE} had a reduced load and time to failure because of extreme generalized corrosion (Figure 4). The surfaces of the alloy 800H tensile specimens were covered by a brown corrosion film and, at 400 mV_{SCE}, by a dark green film. Figures 11 through 14 show that significant general corrosion attack was observed at 400 mV_{SCE}. For the lower applied potential, the attack was observed primarily in the fracture area. The substantial uniform corrosion attack might be overshadowing the presence of incipient or shallow cracks. In order to determine if alloy 800H suffered

TABLE 2
SSRT Conditions and Results for Nickel Alloys

alloy	Test Environment	Applied Potential, mV_{SCE}	Maximum Stress (MPa)	Elongation to Rupture (%)	Reduction of Area (%)	Failure Time (h)	% SCC on Fracture Surface	Results
201	Air, RT	None	414	24.81	89.65	24.99	0	Ductile Failure
	1.1 M $NaHCO_3$ + 1.5 M NaCl, 90°C	400	296	16.87	74.15	19.88	0	Severe general corrosion
		300	313	13.65	67.58	15.85	0	Severe general corrosion
		200	399	28.62	83.77	27.98	0	Severe general corrosion
600	Air, RT	None	723	22.86	59.03	30.33	0	Ductile failure
	1.1 M $NaHCO_3$ + 1.5 M NaCl, 90°C	400	629	22.26	54.75	29.13	>5	SCC
		300	672	18.91	59.50	30.60	>5	SCC
		200	687	28.52	62.07	30.88	0	No SCC
800H	Air, RT	None	568	24.96	49.47	28.53	0	Ductile failure
	1.1 M $NaHCO_3$ + 1.5 M NaCl, 90°C	400	400	11.46	30.52	15.75	0	General corrosion
		300	558	24.94	58.51	28.27	>5	SCC
		200	554	24.64	49.61	27.55	0	No SCC
C-22	Air, RT	None	724	42.65	71.79	58.67	0	Ductile failure
	1.1 M $NaHCO_3$ + 1.5 M NaCl, 90°C	400	518	24.83	49.39	31.00	70	SCC
		300	646	33.96	53.09	48.53	31	SCC
		200	638	42.62	64.12	53.67	0	No SCC

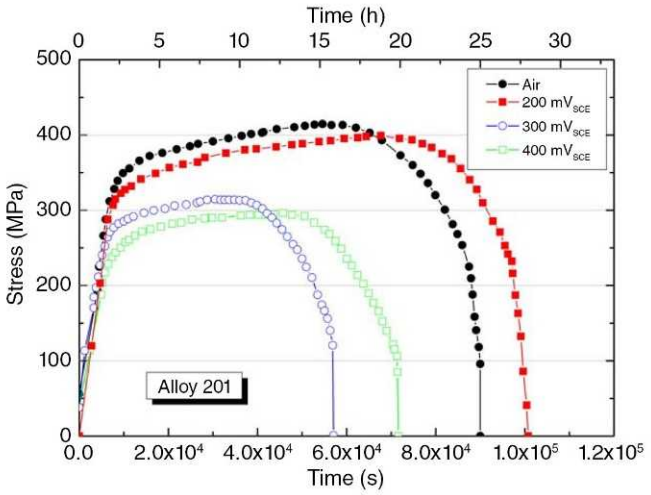

FIGURE 3. *Stress versus time for alloy 201 in air and in a solution containing 1.1 mol/L $NaHCO_3$ + 1.5 mol/L NaCl at 90°C and at applied potentials of 200 mV_{SCE}, 300 mV_{SCE}, and 400 mV_{SCE}.*

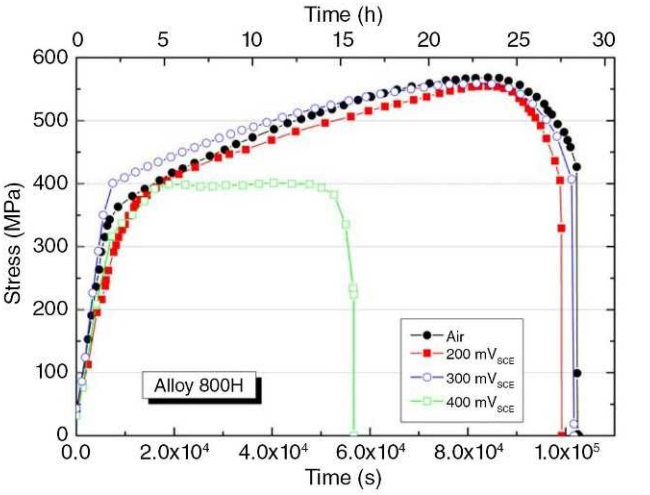

FIGURE 4. *Stress versus time for alloy 800H in air and in a solution containing 1.1 mol/L $NaHCO_3$ + 1.5 mol/L NaCl at 90°C and at applied potentials of 200 mV_{SCE}, 300 mV_{SCE}, and 400 mV_{SCE}.*

from SCC at 300 and 200 mV_{SCE}, the specimens were mounted and polished longitudinally, and observed in an optical microscope. It was found that when the applied potential was 300 mV_{SCE}, alloy 800H showed small cracks.

For alloy 600, a slight decrease of the maximum stress as a function of the applied potential was observed (Figure 5). The failure time decreased only for the test performed at 400 mV_{SCE}. The specimens of alloy 600 did not show significant general corrosion under any of the conditions tested. Only a slight dark gray discoloration on the surface was observed.

Figures 15 to 18 show SEM images of alloy 600 for each tested potential. At all the applied potentials, a significant reduction of area was observed (Figures 15 through 18). The tested specimens were mounted and polished longitudinally, and observed under a microscope looking for cracks. Alloy 600 showed small cracks when strained at 300 and 400 mV (and also perceived in Figures 17 through 18). As in the case of alloy 800H, the SCC of alloy 600 was always accompanied by general corrosion.

Alloy C-22 was the only one that showed long cracks when strained in HCO_3^- and Cl^- solutions at 90°C, and at anodic applied potentials. The stress

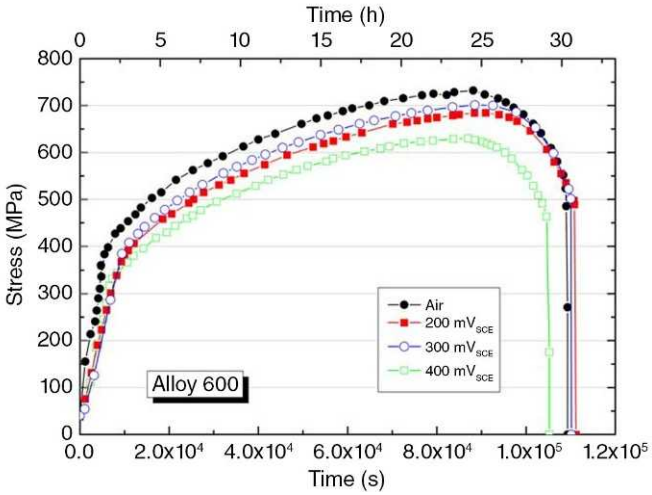

FIGURE 5. *Stress versus time for alloy 600 in air and in a solution containing 1.1 mol/L $NaHCO_3$ + 1.5 mol/L NaCl at 90°C and at applied potentials of 200 mV_{SCE}, 300 mV_{SCE}, and 400 mV_{SCE}.*

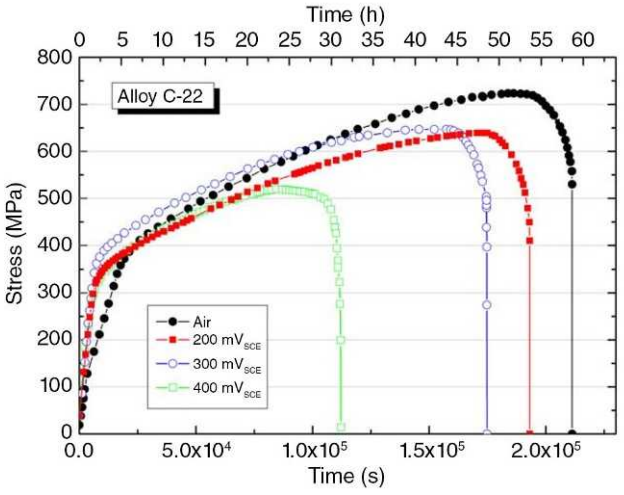

FIGURE 6. *Stress versus time for alloy C-22 in air and in a solution containing 1.1 mol/L $NaHCO_3$ + 1.5 mol/L NaCl at 90°C and at applied potentials of 200 mV_{SCE}, 300 mV_{SCE}, and 400 mV_{SCE}.*

versus time curves showed a marked decrease both in the maximum load and in the rupture time with increasing applied potential (Figure 6). The fracture surface of the specimens, which were tested at potentials of 300 and 400 mV_{SCE}, showed a ductile central area surrounded by a clear brittle transgranular fracture. Furthermore, secondary cracks that run perpendicularly to the applied stress can be clearly distinguished in the body of the tensile specimens (Figures 19 to 22).

Correlation Between the Anodic Peak and the Susceptibility to Cracking—Previous publications linked the SCC susceptibility of alloy C-22 to the presence of an anodic peak during anodic polarization (Figure 1) occurring at potentials below transpassivity in Cl^- and HCO_3^- containing media at temperatures above 60°C.[41]

Current results (Figure 1) showed that alloys C-22, 600, 800H had an anodic peak in potentiodynamic polarization curves in Cl^- containing HCO_3^- solutions.

This peak was more evident in alloys C-22 and 600. Alloy 201 (99.5% Ni) did not show an anodic peak in the range 300 to 400 mV_{SCE}.

From these results, it can be inferred that the anodic peak that occurs in alloy C-22 can be related to the oxidation of one or more of its alloying elements (for example, Cr or Mo). However, because alloy 600 also exhibited the anodic peak and alloy 600 does not contain Mo (Table 1), it is likely that Cr contributes greatly to the anodic peak. It could also be a complex interaction between Ni and Cr (or Ni and Cr + Mo).

Mishra, et al.,[44-45] connected the onset of passive film breakdown to the start of the anodic destruction of the Cr_2O_3-dominated barrier layer to yield the more soluble chromate ($CrO_4^=$). Also, Mishra, et al., showed that the potential breakdown in alloy C-22 is accompanied by the creation of oxidized states of Mo (VI) and W (VI), where W here is tungsten, and they have proposed that the retention of these latter states in the outer regions of the passive film extends the passive region considerably.

In polarization curves obtained in the current work, it is possible to observe that all of the alloys containing Cr (Table 1) present the anodic peak, regardless of the Mo content. So it is assumed that the anodic peak is due to the presence of Cr.

The results of this study show that all the alloys showing the anodic peak in the polarization tests were found to be susceptible to SCC when the applied potential was in the potential range in which this peak appears. Therefore, the presence or not of SCC in alloy C-22 could be connected to the presence of the peak and both (peak and SCC) could be linked to the presence of Cr in the alloy.

As a future work, tensile tests of the same alloys will be performed in pure HCO_3^- solutions to minimize the severe general corrosion produced by the presence of Cl^- ions in some of these alloys. The severe general corrosion interfered with the occurrence of SCC. Eliminating Cl^- from the electrolyte may allow for a more precise conclusion concerning the susceptibility to SCC of Ni-based alloys in HCO_3^- containing solutions.

SUMMARY AND CONCLUSIONS

❖ Potentiodynamic polarization tests show that the alloys C-22, 800H, and 600 have an anodic peak in a range of potential between 200 and 400 mV_{SCE} when tested in HCO_3^- containing media at 90°C. This peak is mainly attributed to the presence of Cr in the alloys.
❖ SSRT showed that only alloy C-22 exhibited a clear case of SCC in 1.1 mol/L $NaHCO_3$ + 1.5 mol/L NaCl at 90°C, and at applied potentials of 300 and 400 mV_{SCE}.
❖ Alloy 201, showed extreme general corrosion,

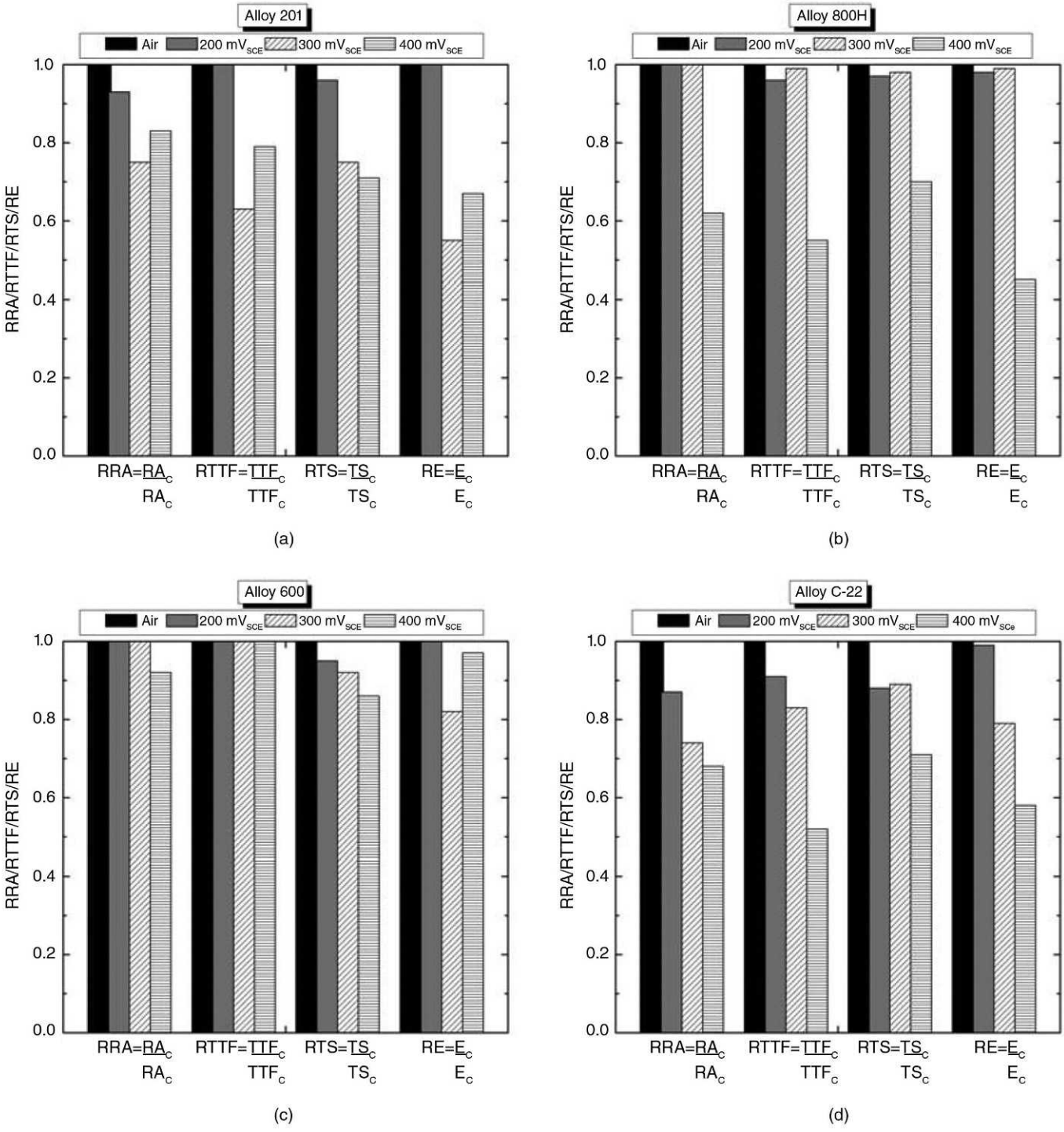

FIGURE 7. *Reduction in area ratio (RRA), time to failure ratio (RTTF), tensile strength ratio (RTS) and elongation ratio (RE) in 1.148 $NaHCO_3$ + 1.5 NaCl solution at 90°C and applied potentials of 200 mV_{SCE}, 300 mV_{SCE}, and 400 mV_{SCE}, for (a) alloy 201, (b) alloy 800H, (c) alloy 600, and (d) alloy C-22.*

making it impossible to conclude if there were cracks after SSRT.

❖ Both alloys 600 and 800H showed small cracks at 300 and 400 mV_{SCE}. Strong general corrosion may compete with the SCC phenomenon.

❖ Current results suggest that all the alloys having an anodic peak in the anodic polarization tests suffer SCC when strained at potentials where the peak appeared. Therefore, the presence of SCC in alloy C-22 could be associated with the presence of the peak, and both (the peak and SCC) could be linked to the presence of Cr in the alloy.

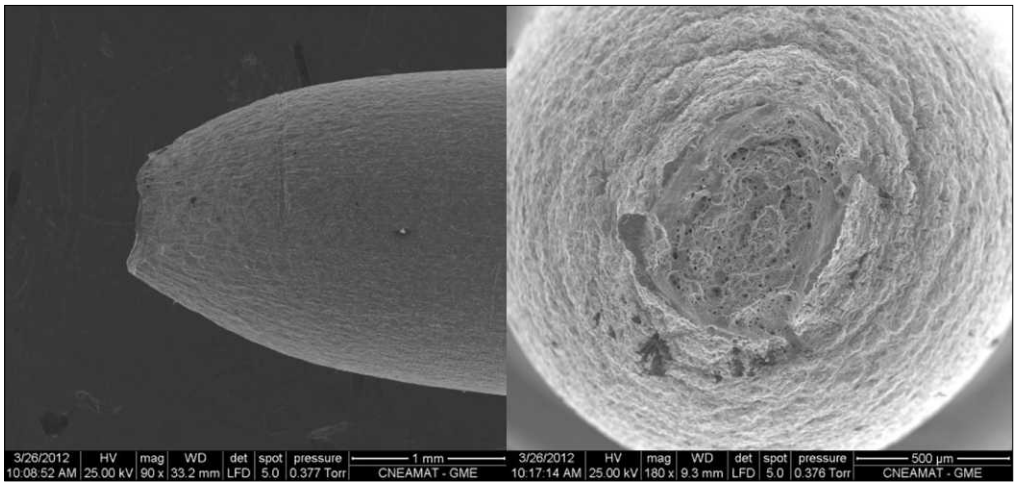

FIGURE 8. *Macrographs of alloy 201, after the tensile test in air. The fracture is ductile with high reduction in area.*

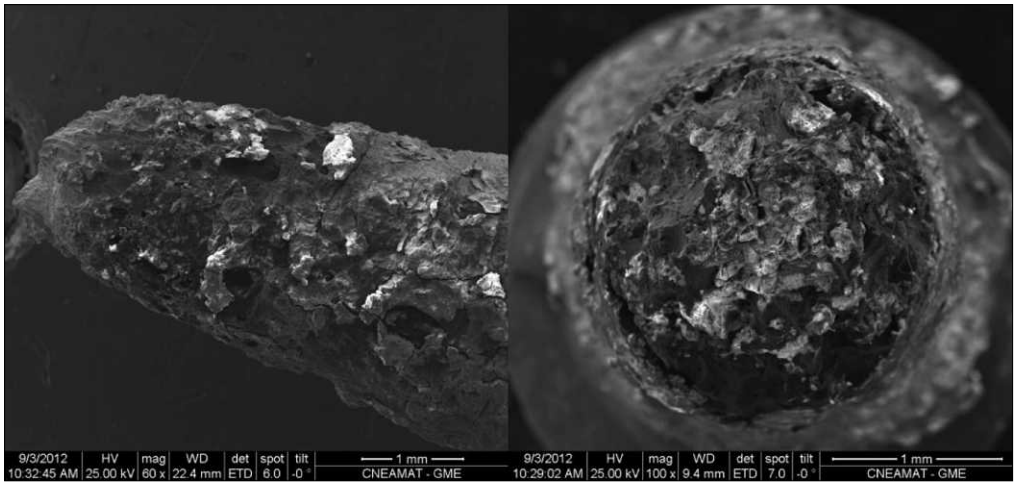

FIGURE 9. *Macrographs of alloy 201, after the tensile test in 1.148 $NaHCO_3$ + 1.5 NaCl solution at 90°C at 300 mV_{SCE}. Severe general dissolution is observed.*

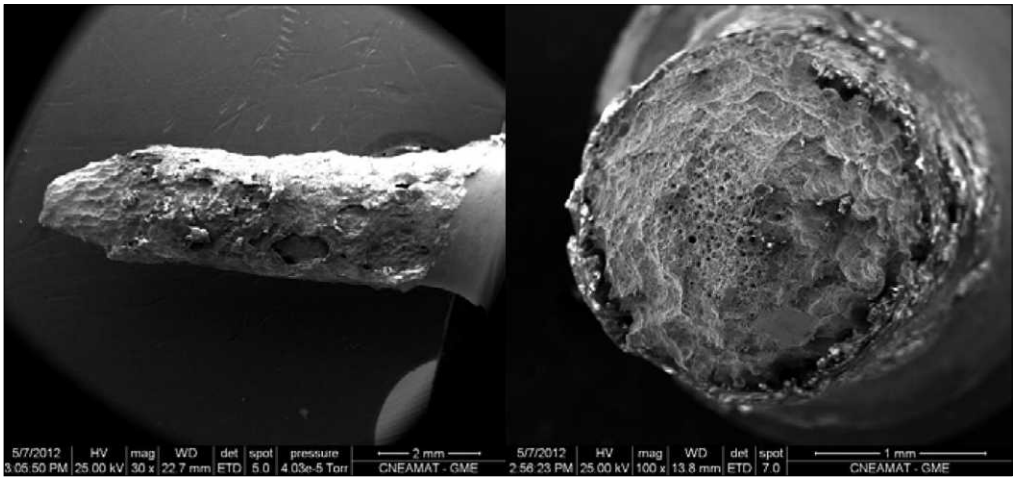

FIGURE 10. *Macrographs of alloy 201, after the tensile test was performed in 1.148 $NaHCO_3$ + 1.5 NaCl solution at 90°C and 400 mV_{SCE}. Severe general corrosion at the high anodic applied potential.*

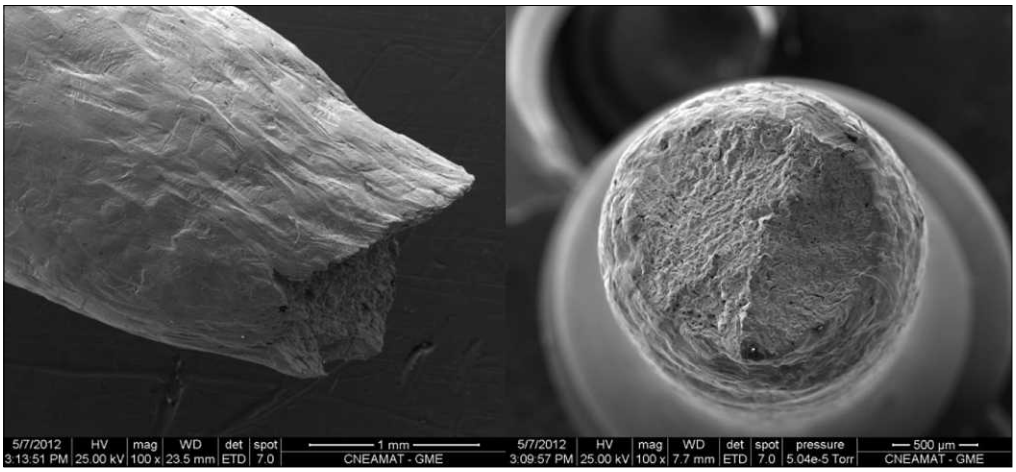

FIGURE 11. *Macrographs of alloy 800H, after the tensile test in air.*

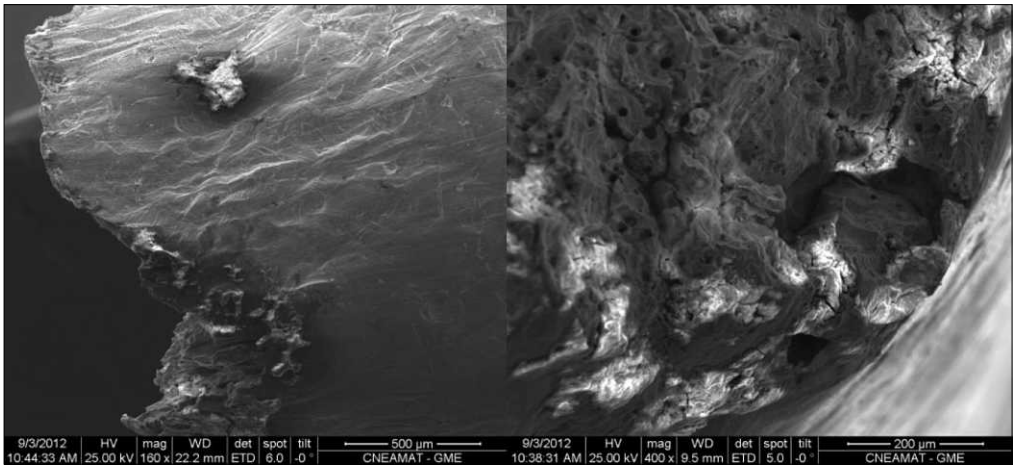

FIGURE 12. *Macrographs of alloy 800H, after the tensile test in 1.148 $NaHCO_3$ + 1.5 NaCl solution at 90°C and 200 mV_{SCE}.*

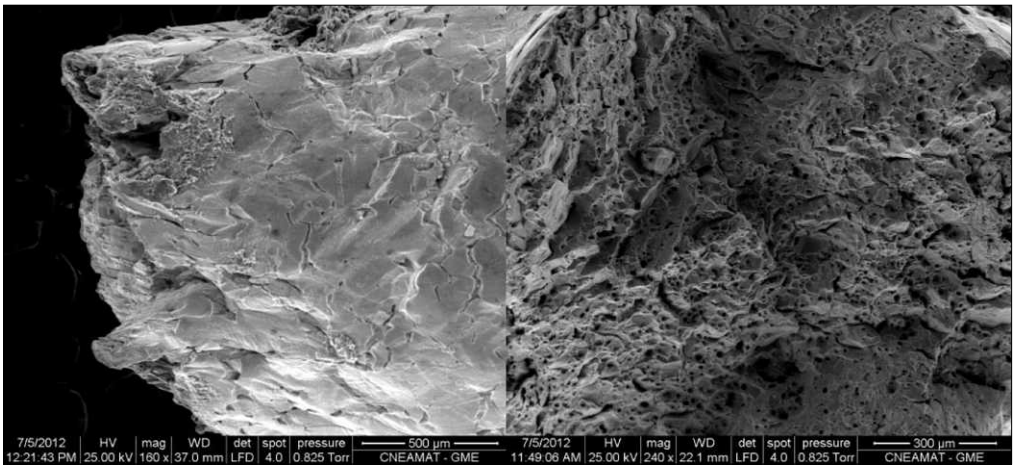

FIGURE 13. *Macrographs of alloy 800H, after the tensile test in 1.148 $NaHCO_3$ + 1.5 NaCl solution at 90°C and at 300 mV_{SCE}. Shallow cracking appeared in the necking area.*

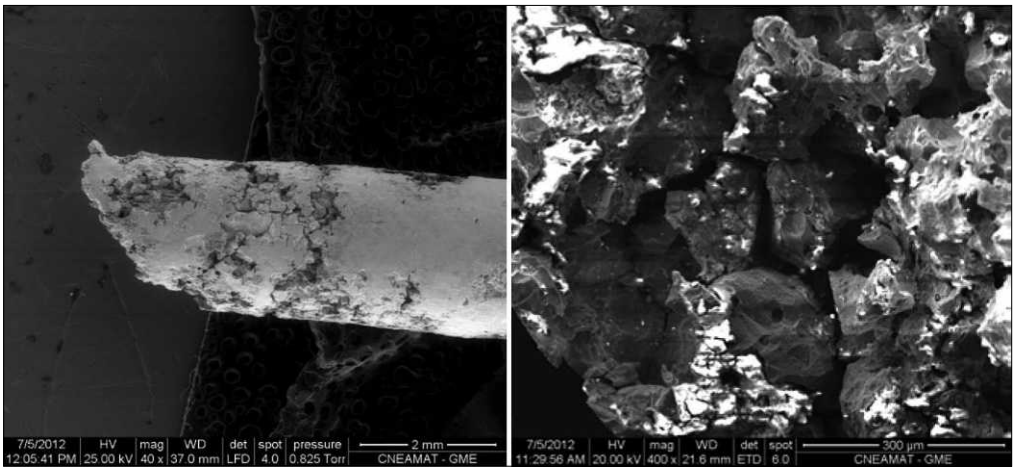

FIGURE 14. *Macrographs of alloy 800H, after the tensile test in 1.148 $NaHCO_3$ + 1.5 NaCl solution at 90°C and at 400 mV_{SCE}. General corrosion plus cracking.*

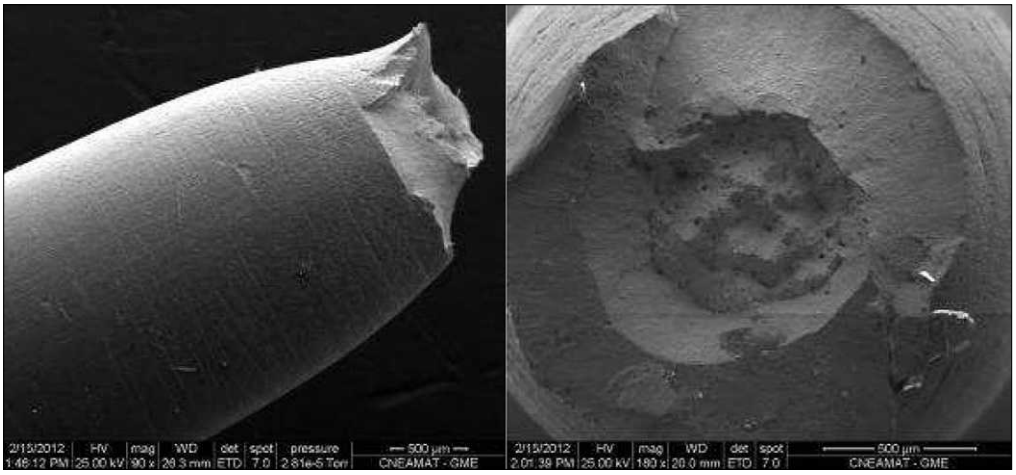

FIGURE 15. *Micrographs of alloy 600 after performed the tensile test in air.*

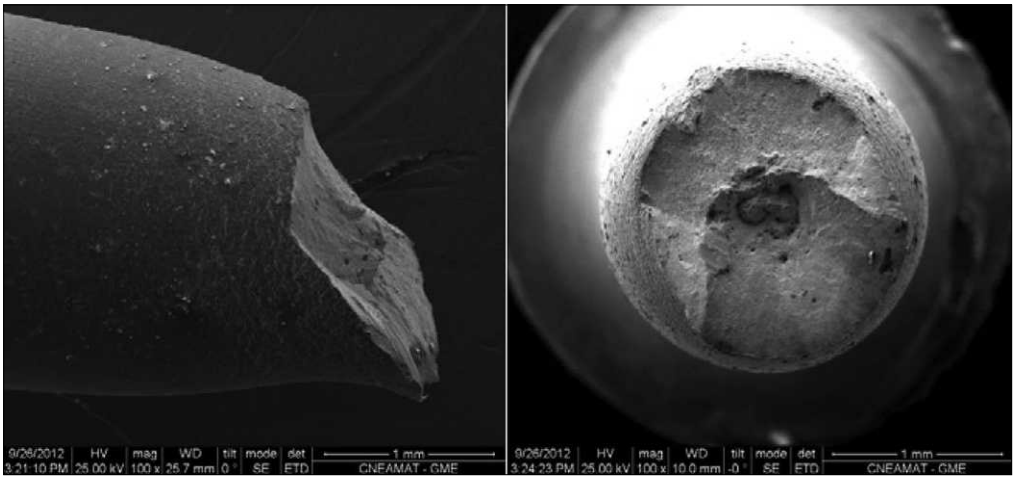

FIGURE 16. *Micrographs of alloy 600, after performed the tensile test in 1.148 $NaHCO_3$ + 1.5 NaCl solution at 90°C and 200 mV_{SCE}.*

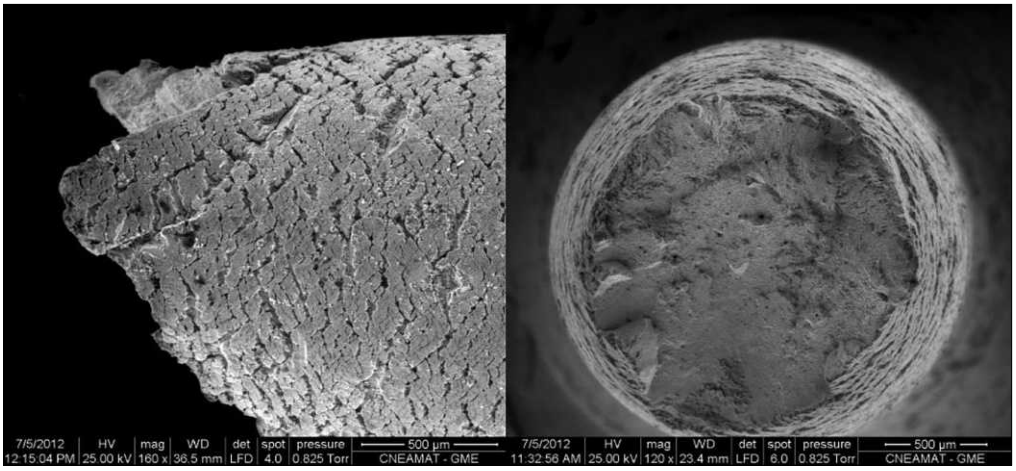

FIGURE 17. *Micrographs of alloy 600, after performed the tensile test in 1.148 $NaHCO_3$ + 1.5 NaCl solution at 90°C in 300 mV_{SCE}.*

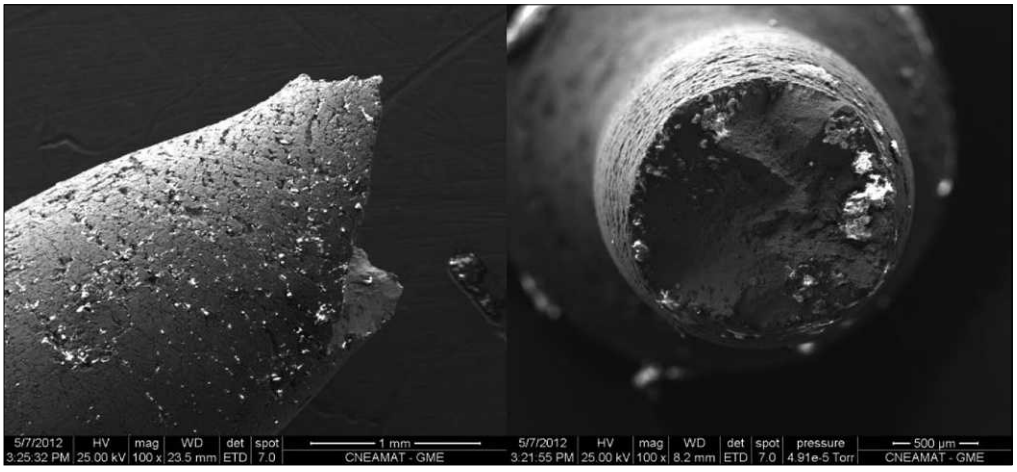

FIGURE 18. *Micrographs of alloy 600, after performed the tensile test in 1.148 $NaHCO_3$ + 1.5 NaCl solution, at 90°C and 400 mV_{SCE}. General corrosion and SCC.*

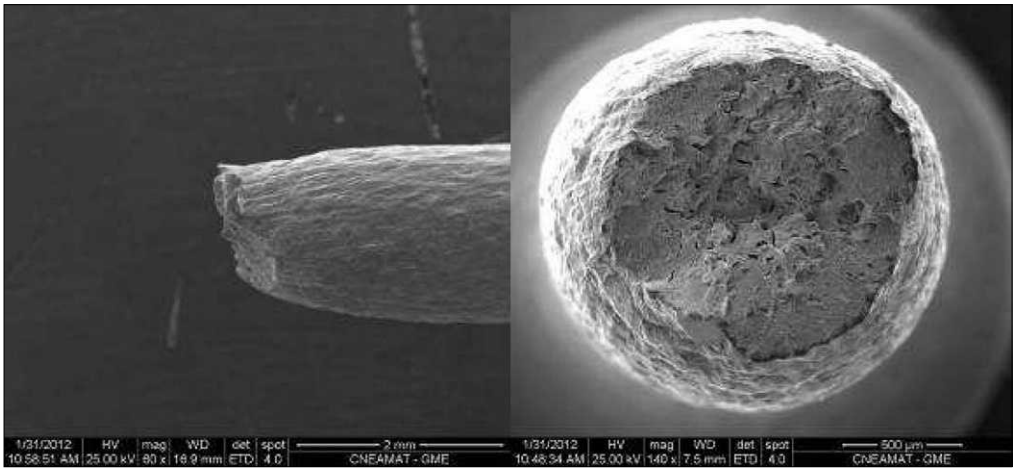

FIGURE 19. *Micrographs of alloy C-22, after the tensile test was performed in air.*

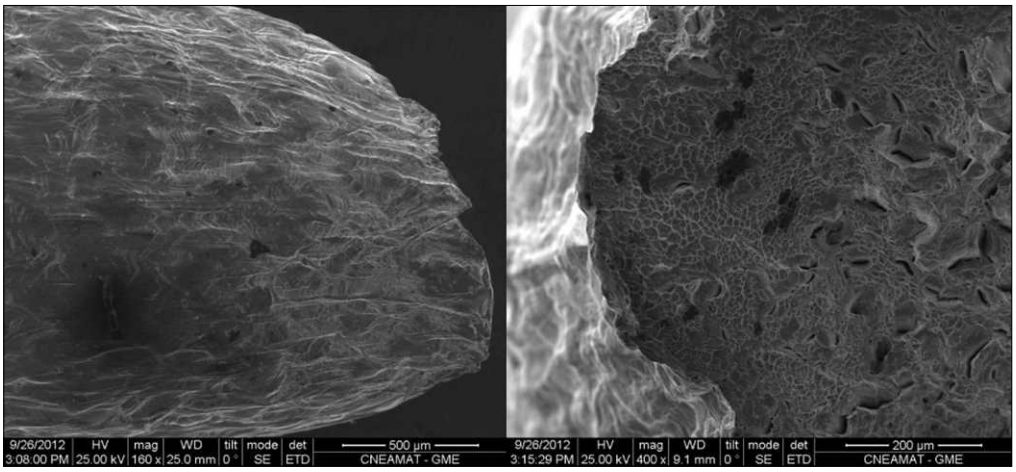

FIGURE 20. *Micrographs of alloy C-22, after the tensile test was performed in 1.148 $NaHCO_3$ + 1.5 NaCl solution, at 90°C and 200 mV_{SCE}. Shallow or no SCC.*

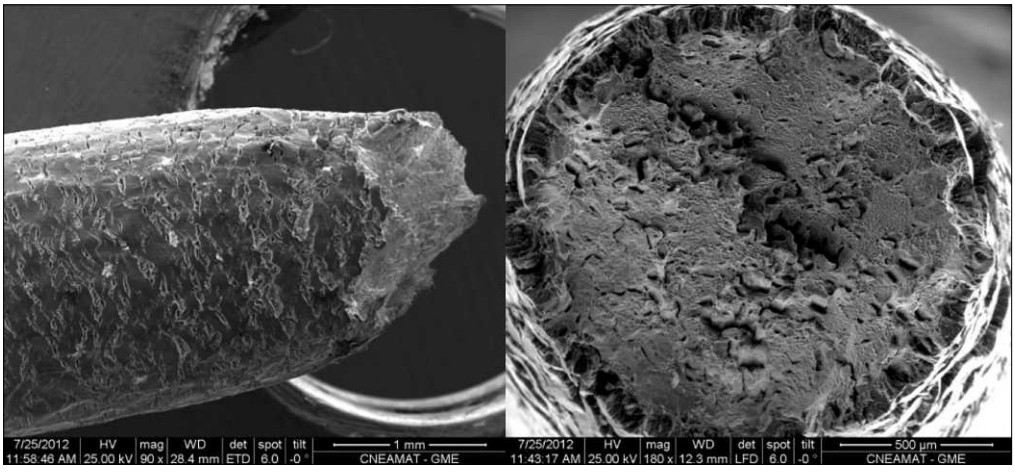

FIGURE 21. *Micrographs of alloy C-22, after the tensile test was performed in 1.148 $NaHCO_3$ + 1.5 NaCl solution at 90°C and 300 mV_{SCE}. SCC is observed.*

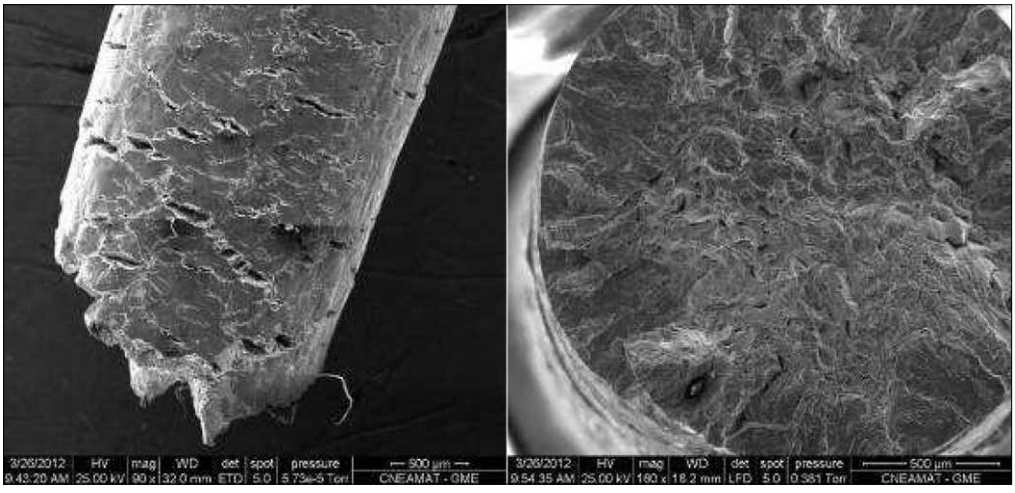

FIGURE 22. *Micrographs of alloy C-22, after the tensile test was performed in 1.148 $NaHCO_3$ + 1.5 NaCl solution, at 90°C and 400 mV_{SCE}. Well defined SCC failure mode.*

REFERENCES

1. R.B. Rebak, "Crystalline alloys: Ni" in *Environmental Degradation of Advanced and Traditional Engineering Materials*, eds. L.H. Hihara, R.P.I. Adler, R.M. Latanision (Boca Raton, FL: CRC Press, Taylor & Francis Group, 2014), p. 197-218.
2. R.B. Rebak, "Stress Corrosion Cracking (SCC) of Nickel-Based alloys," in *Stress Corrosion Cracking, Theory and Practice*, eds. V.S. Raja, Tetsuo Shoji (Cambridge, UK: Woodhead Publishing, 2011), p. 273-306.
3. R.W. Staehle, J.A. Gorman, *Corrosion* 59 (2003): p. 931-994.
4. R.W. Staehle, J.A. Gorman, *Corrosion* 60 (2004): p. 5-63.
5. P.L. Andresen, M.M. Morra *Corrosion* 64, 1 (2008): p. 15-29.
6. K. Arioka, T. Yamada, T. Miyamoto, T. Terachi, *Corrosion* 67, 3 (2011): p. 035006-1 to 035006-18.
7. X. Ru, R.W. Staehle, *Corrosion* 69, 3 (2013): p. 211-229.
8. P.L. Andresen, *Corrosion* 69, 10 (2013): p. 1024-1038.
9. A. Hojná, *Corrosion* 69, 10 (2013): p. 964-974.
10. S.M. Bruemmer, M.J. Olszta, M.B. Toloczko, L.E. Thomas, *Corrosion* 69, 10 (2013): p. 953-963.
11. K. Arioka, T. Yamada, T. Miyamoto, M. Aoki, *Corrosion* 70, 7 (2014): p. 695-707.
12. M. Iannuzzi, "Environmentally Assisted Cracking (EAC) in Oil and Gas Production," in *Stress Corrosion Cracking, Theory and Practice*, eds. V.S. Raja, Tetsuo Shoji (Cambridge, UK: Woodhead Publishing, 2011), p. 570-607.
13. J.R. Scully, W.R. Cieslak, F.S. Bovard, *J. Electrochem. Soc.* 138, 8 (1991): p. 2229-2237.
14. J.A. Wasynczuk, M.V. Quinzio, H.F. Bittner, *J. Electrochem. Soc.* 142, 9 (1995): p. 2977-2985.
15. T.S.F. Lee, R.M. Latanision, *Metall. Mater. Trans. A* 18A, 9 (1987): p. 1653-1662.
16. M.L. Martin, B.P. Somerday, R.O. Ritchie, P. Sofronis, I.M. Robertson, *Acta Mater.* 60 (2012): 2739–2745.
17. R.B. Rebak, J.R. Dillman, P. Crook, C.V.V. Shawber, *Mater. Corros.* 52, 4 (2001): p. 289-297.
18. S.J. Pawel, *Corrosion* 50, 12 (1994): p. 963-971.
19. R.B. Rebak, "Environmentally Assisted Cracking in the Chemical Process Industry: Stress Corrosion Cracking of Iron, Nickel, and Cobalt Based Alloys in Chloride and Wet HF Services," in *Environmentally Assisted Cracking: Predictive Methods for Risk Assessment and Evaluation of Materials, Equipment and Structures*, ASTM STP 1401 (West Conshohocken, PA: ASTM, 2000), p. 289.
20. R.B. Rebak, "Metallurgical Effects on the Corrosion Behavior of Nickel Alloys," *ASM Metals Handbook*, Vol. 13A, Corrosion: Fundamental, Testing, and Protection (ASM International, 2003), p. 279-286.
21. Hastelloy C-22 Alloy, Haynes International, brochure H-2019F, 2002.
22. A.I. Asphahani, *Arabian J. Sci. Eng.* (1989), p. 317-335.
23. H.M. Tawancy, R.B. Herchenroeder, A.I. Asphahani, High-Performance Ni-Cr-Mo-W Alloys, J. Metals (1983), p. 37-43.
24. P.A. Whiterspoon, G.S. Bodvarsson, eds. *Geological Challenges in Radioactive Waste Isolation. Third Worldwide Review* (Berkeley, CA: University of California, 2001).
25. K.D. Crowley, J.F. Ahearne, *Am. Sci.* 90, 6 (2002): p. 514.
26. Yucca Mountain Project, eds. G.S. Bodvarsson, C.K. Ho, B.A. Robinson, (Berkeley, CA: Elsevier, 2003).
27. Yucca Mountain Science and Engineering Report, U.S. Department of Energy, Office of Civilian Radioactive Waste Management, DOE/RW-0539, Las Vegas, NV (2001).
28. G.M. Gordon, *Corrosion* 58, 10 (2002): p. 811.
29. R.B. Rebak, "Materials in Nuclear Waste Disposition," *JOM* 3 (2014): p. 455.
30. D.W. Shoesmith, *Corrosion* 62 (2006): p. 703.
31. F. King, *JOM* 3 (2014): p. 526.
32. J.C. Estill, K.J. King, D.V. Fix, D.G. Spurlock, G.A. Hust, S.R. Gordon, R.D. McCright, G.M. Gordon, R.B. Rebak, "Susceptibility of Alloy 22 to Environmentally Assisted Cracking in Yucca Mountain Relevant Environments," CORROSION/2002, paper no. 02535 (Houston, TX: NACE International, 2002).
33. D.S. Dunn, Y.M. Pan, G.A. Cragnolino, "Stress Corrosion Cracking of Nickel-Chromium-Molybdenum Alloys in Chloride Solutions," CORROSION/2002, paper no. 02425 (Houston, TX: NACE, 2002).
34. P.L. Andresen, P.W. Emigh, L.M. Young, G.M. Gordon, "Stress Corrosion Cracking Growth Rate Behavior of Alloy 22 (UNS N06022) in Concentrated Groundwater," CORROSION/2003, paper 0368 (Houston, TX: NACE, 2003).
35. D.V. Fix, J.C. Estill, G.A. Hust, K.J. King, S.D. Day, R.B. Rebak, "Influence of Environmental Variables on the Susceptibility of Alloy 22 to Environmentally Assisted Cracking," CORROSION/2003, paper no. 03688 (Houston, TX: NACE, 2003).
36. V. Fix, J.C. Estill, G.A. Hust, L.L. Wong, R.B. Rebak, "Environmentally Assisted Cracking Behavior of Nickel-Alloys in Simulated Acidified and Alkaline Waters Using U-Bend Specimens," CORROSION/2004, paper no. 04549 (Houston, TX: NACE, 2004).
37. K.J. King, L.L. Wong, J.C. Estill, and R.B. Rebak, "Slow Strain Rate Testing of alloy 22 in Simulated Concentrated Ground Waters," Paper No. 04548, CORROSION 2004, NACE International, Houston, Texas, 2004.
38. K.T. Chiang, D.S. Dunn, G.A. Cragnolino, "Effect of Groundwater Chemistry on Stress Corrosion Cracking," CORROSION/2005, paper no. 05463 (Houston, TX: NACE, 2005).
39. K.T. Chiang, D.S. Dunn, G.A. Cragnolino, "Combined Effect of Bicarbonate and Chloride Ions on Stress Corrosion Cracking Susceptibility of Alloy 22," CORROSION/2006, paper no. 06506 (Houston, TX: NACE, 2006).
40. K.T. Chiang, D.S. Dunn, G.A. Cragnolino, "Effect of Simulated Groundwater Chemistry on Stress Corrosion Cracking of Alloy 22," *Corrosion* 63, 10 (2007): p. 940-950.
41. P.K. Shukla, D.S. Dunn, K.-T. Chiang, O. Pensado, "Stress Corrosion Cracking Model for Alloy 22 in the Potential Yucca Mountain Repository Environment," CORROSION/2006, paper no. 06502 (Houston, TX: NACE, 2006).
42. D.S. Dunn, Y.-M. Pan, K.T. Chiang, G.A. Cragnolino, "Surface Analysis of Alloy 22 Under Conditions That Promote Stress Corrosion Cracking," CORROSION/2006, paper no. 06509 (Houston, TX: NACE, 2006).
43. R.B. Rebak, *Corrosion* 65, 4 (2009): p. 252-271.
44. A.K. Mishra, S. Ramamurthy, M. Biesinger, D.W. Shoesmith, *Electrochimica Acta* 100 (2013): p. 118-124.
45. A.K. Mishra, D.W. Shoesmith, *Electrochim. Acta* 102 (2013): p. 328-335.
46. ASTM G5-94 (2004), "Standard Reference Test Method for Making Potentiostatic and Potentiodynamic Anodic Polarization Measurements," in *Annual Book of ASTM Standards*, vol. 03.02 (West Conshohocken, PA: ASTM International, 2004), p. 53-64.
47. D.D. Macdonald, A.C. Scott, P. Wentrcek, *J. Electrochem. Soc.* 126 (1978): p. 908.
48. ASTM G129 (2004), "Standard Practice for Slow Strain Rate to Evaluate the Susceptibility of Metallic Materials to Environmentally Assisted Cracking," in *Annual Book of ASTM Standards*, vol. 03.02 (West Conshohocken, PA: ASTM International, 2004), p. 552-558.
49. M. Pourbaix, *Atlas of Electrochemical Equilibria in Aqueous Solutions* (Houston, TX: NACE, Cebelcor, 1974).